Taylor & Francis
Taylor & Francis Group

RESEARCH PAPER

Check for updates

MED1 mediator subunit is a key regulator of hepatic autophagy and lipid metabolism

Jin Zhou[a], Brijesh K. Singh[a], Jia Pei Ho[a], Andrea Lim[a], Eveline Bruinstroop [b], Kenji Ohba [a], Rohit A. Sinha[a,c], and Paul M. Yen[a,d]

[a]Program of Cardiovascular & Metabolic Disorders, Duke-NUS Medical School Singapore, Singapore; [b]Department of Endocrinology and Metabolism, Amsterdam UMC, Amsterdam, The Netherlands; [c]Department of Endocrinology, Sanjay Gandhi Postgraduate Institute of Medical Sciences, Lucknow India; [d]Duke Molecular Physiology Institute and Department of Medicine, Duke University Medical Center, Durham, NC USA

ABSTRACT

Hepatic macroautophagy/autophagy and fatty acid metabolism are transcriptionally regulated by nuclear receptors (NRs); however, it is not known whether their transcriptional co-activators are involved in autophagy. We thus examined MED1 (mediator complex subunit 1), a key component of the Mediator Complex that directly interacts with NRs, on these processes. We found that *MED1* knockdown (KD) in cultured hepatic cells decreased autophagy and mitochondrial activity that was accompanied by decreased transcription of genes involved in these processes. Lipophagy and fatty acid β-oxidation also were impaired. These effects also occurred after thyroid hormone stimulation, nutrient-replete or -deplete conditions, and in liver-specific *Med1* KD (*Med1* LKD) mice under fed and fasting conditions. Together, these findings showed that *Med1* played a key role in hepatic autophagy, mitochondria function, and lipid metabolism under these conditions. Additionally, we identified downregulated hepatic genes in *Med1* LKD mice, and subjected them to ChIP Enrichment Analysis. Our findings showed that the transcriptional activity of several NRs and transcription factors (TFs), including PPARA and FOXO1, likely were affected by *Med1* LKD. Finally, *Med1* expression and autophagy also were decreased in two mouse models of nonalcoholic fatty liver disease (NAFLD) suggesting that decreased *Med1* may contribute to hepatosteatosis. In summary, *MED1* plays an essential role in regulating hepatic autophagy and lipid oxidation during different hormonal and nutrient conditions. Thus, *MED1* may serve as an integrator of multiple transcriptional pathways involved in these metabolic processes.

Abbreviations: BAF: bafilomycin A$_1$; db/db mice; *Lepr*$^{db/db}$ mice; ECAR: extracellular acidification rate; KD: knockdown; MED1: mediator complex subunit 1; NAFLD: nonalcoholic fatty liver disease; OCR: oxygen consumption rate; PPARA/PPARα: peroxisomal proliferator activated receptor alpha; TF: transcription factor; TFEB: transcription factor EB; tf-LC3: tandem fluorescence RFP-GFP-LC3; TG: triglyceride; TH: Thyroid hormone; TR: thyroid hormone receptors; V-ATPase: vacuolar-type H$^+$-ATPase; WDF: Western diet with 15% fructose in drinking water

Introduction

Autophagy is a highly conserved cellular process that degrades intracellular components by autophagosome engulfment of various intracellular cargos, followed by fusion with lysosomes to form autolysosomes, and lysosomal degradation of its contents [1,2]. This process plays an important role in maintaining energy homeostasis by degrading macromolecules such as lipid droplets, glycogen, and proteins to provide substrates for cellular metabolism [3].

During periods of starvation, cells shift their metabolism from glucose metabolism to fatty acid oxidation to produce energy [4,5]. In the liver, autophagy is activated by starvation, and preferentially degrades intrahepatic lipid droplets to release free fatty acids for mitochondrial β-oxidation [6,7], a process also termed as lipophagy. Loss of lipophagy impairs the mobilization of triglycerides from lipid droplets and

results in hepatosteatosis [6,7]. This connection between autophagy and lipid metabolism is further demonstrated by their co-regulation during starvation or in response to hormonal stimuli [8–11]. For example, starvation activates TFEB (transcription factor EB) to initiate the transcription of autophagy and lysosomal genes [12,13], as well as genes for lipid metabolism [14]. The nuclear receptor PPARA/PPARα (peroxisomal proliferator activated receptor alpha) plays a critical role in nutrient-sensing, and regulates hepatic autophagy and lipid metabolism during fasting and feeding cycles [15,16]. Thyroid hormone (TH) binding to thyroid hormone receptors (TRs) also increases autophagy and mitochondrial lipid oxidation [7,17,18]. Currently, little is known about the role of transcriptional co-activators on autophagy and lipid metabolism during starvation or hormone stimulation.

MED1 (mediator complex subunit 1) is a major component of the multi-subunit mediator complex that bridges

transcription factors (TFs) or nuclear receptors (NRs) bound to promoter enhancer elements with RNA polymerase II and the general transcriptional machinery. As such, it serves as a co-activator to increase the transcription of target genes [19]. *MED1* directly binds to multiple NRs, including thyroid hormone receptors (TRs) [20], through its two LXXLL motifs. Currently, it is not known whether *MED1* is involved in the regulation of autophagy during starvation or hormone stimulation. In the current study, we demonstrate that loss of *MED1* not only regulated these processes during nutrient-replete and starvation conditions but also decreased T_3-stimulated autophagy, β-oxidation, and lipid clearance. Liver-specific KD of *MED*1 also decreased the transcription of autophagic and mitochondrial genes. *Med1* expression and autophagy also were decreased in two mouse models of non-alcoholic fatty liver disease (NAFLD). Taken together, these results suggest that *MED1* is an important modulator of hepatic autophagy, β-oxidation, and lipid clearance, and also may modify the severity of NAFLD by its effects on autophagy and mitochondrial function.

Results

MED1 *KD decreases autophagy in hepatic cells*

To investigate the role of *MED1* on hepatic autophagy, we employed *MED1* siRNA to knock down its endogenous expression in HepG2 human hepatoma cells, which retain many liver-specific metabolic functions [21]. Knockdown of *MED1* did not affect the viability or cell number of these cells (Fig. S1). Western blotting showed that siRNA knockdown (KD) of *MED1* decreased the protein level of autophagosome marker MAP1LC3B/LC3B-II (Figure 1A). *MED1* KD also decreased the number of eGFP-LC3B puncta in cells transfected with this plasmid suggesting there was less autophagosome formation thereby a decrease in autophagy (Fig. S2). Furthermore, immunofluorescence staining for endogenous MAP1LC3B further confirmed that there was decreased autophagosome number in *MED1* KD cells (Figure 1B).

SQSTM1/p62 is an ubiquitin-binding scaffold protein that binds to ubiquitinated protein aggregates and accumulates when autophagic flux is inhibited [22]. In *MED1* KD cells, we observed increased SQSTM1 protein (Figure 1A). In conjunction with decreased MAP1LC3B-II, these data suggested that autophagic flux was decreased by *MED1* KD. We then examined the accumulation of MAP1LC3B-II in the presence of bafilomycin A_1 (Baf), a V-ATPase (vacuolar-type H^+-ATPase) inhibitor that neutralizes lysosomal acidity to inhibit the lysosomal/autolysosomal degradation [23]. As shown in Figure 1C, we observed a smaller induction of MAP1LC3B-II levels in *MED1* KD cells than control cells after Baf treatment, indicating there was a decrease in autophagic flux in *MED1* KD cells. To eliminate the possibility of off-target effects affecting autophagy, we tested 3 individual siRNAs that targeted human *MED1* in HepG2 cells, and consistently observed decreased autophagic flux (Fig. S3).

Similar results also were observed in immortalized mouse AML-12 hepatic cells (Fig. S4).

We further analyzed autophagy flux by transfecting control and *MED1* KD HepG2 cells with a tandem fluorescence RFP-GFP-LC3 (tf-LC3) plasmid [24]. In this assay, dual fluorescence of both GFP and RFP tagged to LC3 occurred in autophagosomes whereas the single fluorescence from RFP occurred only in autolysosomes since GFP was denatured in the acidic autolysosome environment. Thus, in the overlaid images, yellow dots represented autophagosomes, and red dots represented autolysosomes. Using this assay, we observed decreases in the amounts of both autophagosomes (yellow dots) and autolysosomes (red dots) in *MED1* KD cells (Figure 1D). Interestingly, the ratio of red to yellow puncta was not significantly different. Taken together, our results demonstrated that *MED1* KD decreased autophagy flux by reducing autophagosome formation.

MED1 *KD decreases oxidative phosphorylation and fatty acid β-oxidation and in hepatic cells*

Because *MED1* is a transcriptional coactivator, we next examined its role in the transcriptional regulation of several key autophagy genes. *MED1* KD decreased *MAP1LC3B*, *SQSTM1/p62*, and *VAMP7* mRNA levels (Figure 2A). Interestingly, the mRNA levels of two important regulators of mitochondrial fatty acid β-oxidation, *PPARA*, and PPARGC1A/PGC1α, and several other mitochondrial genes also were decreased (Figure 2B). To assess the net effect of *MED1* KD on cellular oxidative and glycolytic function, we used Seahorse XF Cell Energy Phenotype Test Kit to examine oxygen consumption rate (OCR) and extracellular acidification rate (ECAR). Control cells had a greater increase in OCR than *MED1* KD cells, suggesting that *MED1* KD cells had compromised oxidative function (Figure 2C). Analyses of metabolic potential as a percentage of baseline showed a decrease in OCR in *MED1* KD cells compared to control cells (Figure 2C). Interestingly, glycolytic potential did not significantly change in both control and *MED1* KD cells during stress condition since no change of ECAR was observed. These findings demonstrated that *MED1* KD decreased mitochondrial function but did not affect glycolytic function. We further assessed the effect of *MED1* KD on mitochondrial function using the Mito Stress test. *MED1* KD decreased mitochondrial basal respiration, ATP turnover, and maximum respiratory capacity (Figure 2D), further confirming that *MED1* KD led to a decreased mitochondrial activity. To determine the effects of *MED1* KD on mitochondrial fatty acid oxidation, we next measured cellular OCR before and after addition of the CPT1α inhibitor, Etomoxir, which blocks acylcarnitine uptake into mitochondria and inhibits β-oxidation; thus, the decrease in OCR is an indicator of mitochondrial fatty acid β-oxidation. *MED1* KD cells had lower basal OCR as well as less reduction in OCR after Etomoxir treatment when compared with control cells under similar conditions (Figure 2E), indicating there was decreased fatty acid oxidation in *MED1* KD cells compared to control cells. Consistent with these
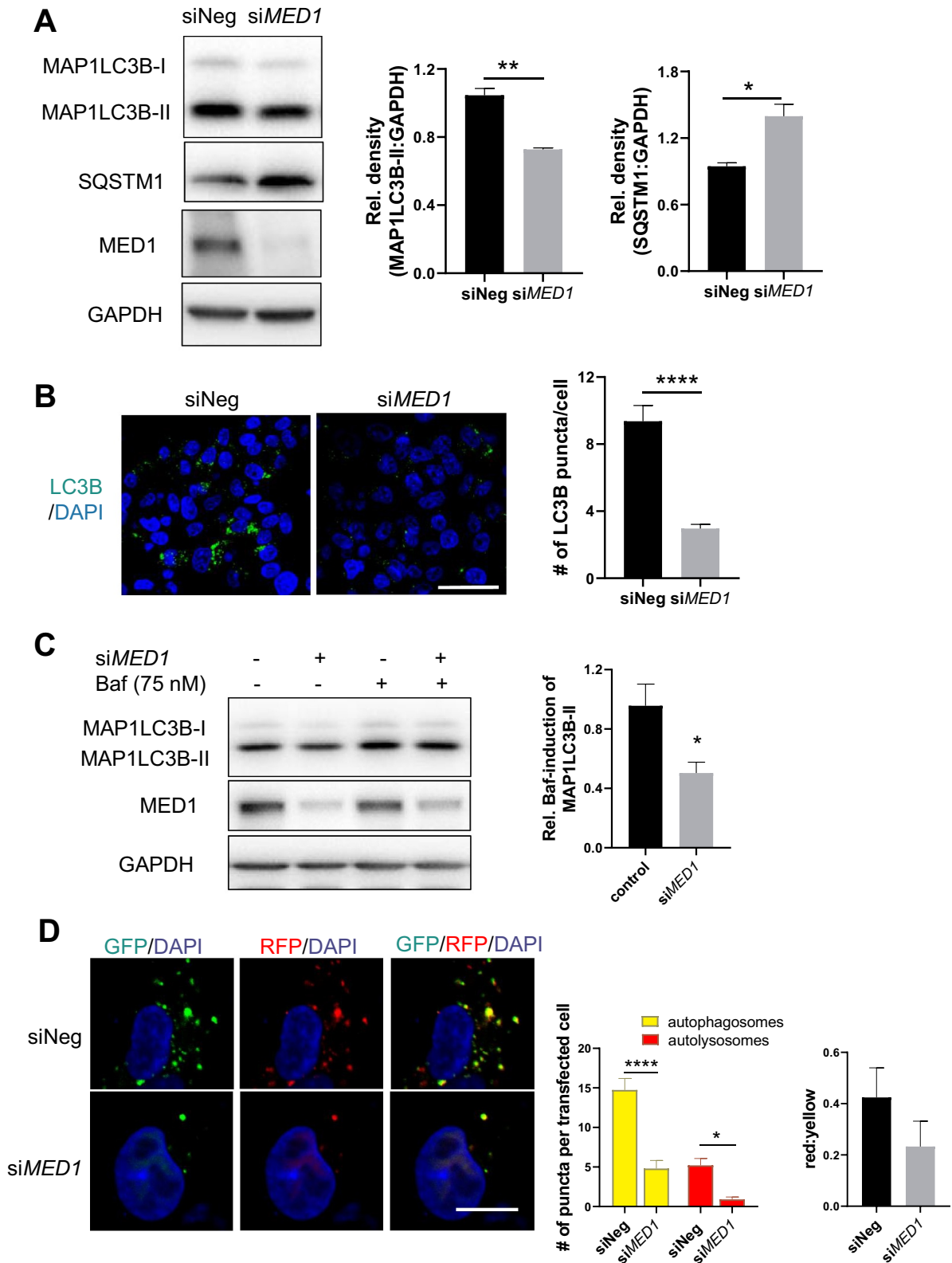
Figure 1. siRNA KD of *MED1* decreased autopahgy in HepG2 cells. (A) Immunoblot and densitometric analysis showing that 48 h after siRNA (10 nM) KD of MED1 decreased MAP1LC3B-II and increased SQSTM1. Bars represent the mean of the respective individual ratios ± SEM (n = 3). (B) MAP1LC3B immunostaining showing decreased endogenous MAP1LC3B puncta in *MED1* KD cells. Scale bar: 50 μm. MAP1LC3B puncta/per cell were counted. Bars represent the mean ± SEM (n = 30) (C) Evaluation of autophagy flux in HepG2 cells using lysosomal inhibitor bafilomycin A_1 (Baf, 150 nM). Baf-induced accumulation of MAP1LC3B-II in control or *MED1* siRNA transfected cells were represented as mean ± SEM (n = 3). (D) Quantification and representative image of autophagosomes (yellow puncta on overlay) and autolysosomes (RFP puncta on overlay) in tandem RFP/GFP-tagged MAP1LC3B plasmid-transfected HepG2 cells with or without *MED1* KD. Yellow and red puncta per transfected cells were counted, and the ratio of yellow to red puncta were calculated. Scale bar: 10 μm. Data are represented as mean ± SEM (n ≥ 10).
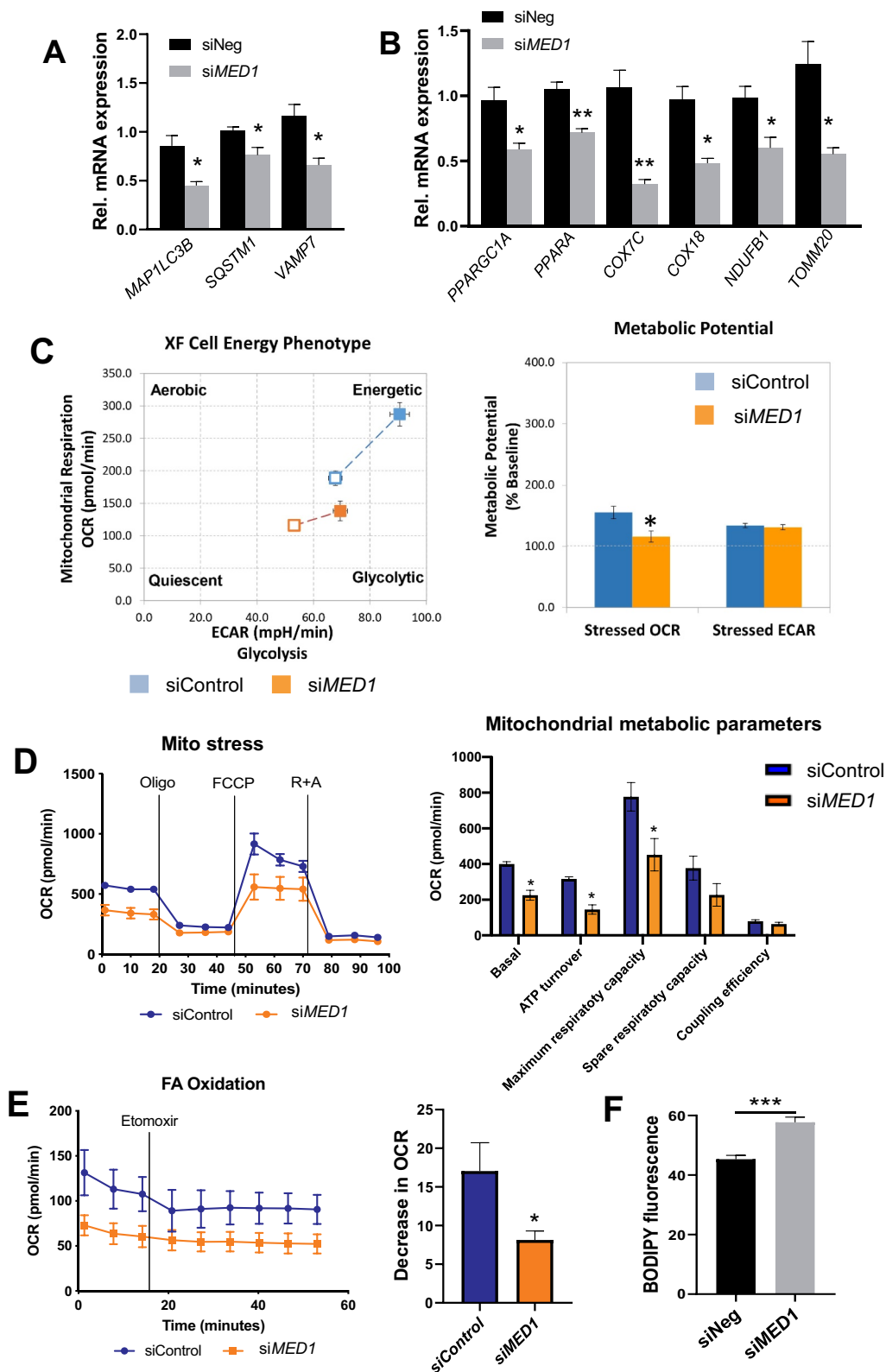
Figure 2. siRNA KD of *MED1* decreased fatty acid oxidation, oxidative phosphorylation and lipid clearance in HepG2 cells. Assays were performed 48 h after siRNA transfection. (A) KD of *MED1* decreased mRNA expression of autophagic genes. Bars represent the mean ± SEM (n = 3). (B) KD of *MED1* decreased mRNA expression of key metabolic and mitochondrial genes. Bars represent the mean ± SEM (n = 3). (C). Seahorse XF cell energy phenotype test showed that KD of *MED1* decreased metabolic bioenergetics and oxidative potential. Bars represent the mean ± SEM (n = 12). (D) Seahorse XF Mito Stress Test showed that KD of *MED1* decreased oxygen consumption rate (OCR) and mitochondrial metabolic potential in HepG2 cells. Data are presented as mean ± SEM (n = 12). (E) Seahorse XF Fatty Acid (FA) Oxidation test showed decreased fatty acid oxidation in *MED1* KD HepG2 cells. Data are presented as mean ± SEM (n = 12). (F) KD of *MED1* increased cellular neutral lipid content in HepG2 cells. Lipid droplets was stained with BODIPY 493/503 (5 μg/ml), and measured by flow cytometry. Data are represented as mean ± SEM (n = 3).

findings, we also observed a small, but significant, reciprocal increase in intracellular lipid content in *MED1* KD cells compared to cells transfected with control siRNA under basal conditions (Figure 2F).

MED1 KD decreases induction of autophagy, lipophagy, oxidative phosphorylation, and target gene expression by T$_3$ in hepatic cells

We previously reported that T$_3$ stimulated hepatic autophagy of lipids from fat droplets (lipophagy) to increase β-oxidation of fatty acids [7,25]. Since *MED1* is an important co-activator for TRs, we examined whether T$_3$ could stimulate autophagy after *MED1* KD in hepatic cells. Interestingly, *MED1* KD abrogated stimulation of MAP1LC3B-II expression by T$_3$ (Figure 3A). We next investigated whether stimulation of lipophagy by T$_3$ was modulated by *MED1*, and found that T$_3$ treatment of control siRNA-transfected cells had significantly more colocalization of BODIPY and LysoTracker staining than T$_3$ treatment of *MED1* KD cells (yellow puncta, Figure 3B), indicating that *MED1* KD decreased the lipophagy induced by T$_3$. We analyzed the expression of several target genes stimulated by T$_3$: *PPARGC1A, CPT1A*, and *MAP1LC3B*, which are involved in mitochondrial biogenesis and function, fatty acid entry into mitochondria, and autophagy, respectively, and found that *MED1* KD blunted transcriptional induction of these genes by T$_3$ (Figure 3C). Finally, we examined stimulation of OCR by T$_3$ in HepG2 cells, and found that *MED1* KD abrogated the stimulation of basal respiration, ATP turnover, maximum respiratory capacity, and spare respiratory capacity induced by T$_3$ (Figure 3D). Taken together, these results showed that T$_3$-mediated autophagy/lipophagy and oxidative phosphorylation was abolished by *MED1* KD.

MED1 KD decreases autophagy, lipophagy, and fatty acid oxidation induced by starvation in hepatic cells

During starvation, induction of autophagy promotes the breakdown of lipid droplets and the release of free fatty acid for mitochondrial β-oxidation to generate ATP. Thus, we investigated whether *MED1* played a role in stimulating autophagy and lipid catabolism in hepatic cells during starvation. Fluorescence imaging of HepG2 cells transfected with tf-LC3 plasmid which expressed both green and red fluorescent proteins showed more yellow puncta (autophagosomes) than red puncta (autolysosomes) in full medium (Figure 4A). There also was an increase in the ratio of red to yellow puncta after HBSS starvation (Figure 4B). In full medium, *MED1* KD cells had a similar puncta pattern as HepG2 cells but at much lower levels. In contrast to HepG2 control cells, *MED1* KD cells did not show any change in the ratio of red to yellow puncta after starvation (Figure 4B). These data suggested that there was decreased levels of autophagosomes and autolysosomes after *MED1* KD as well as decreased autophagic flux during starvation. These findings were further confirmed by the abrogation of the bafilomycin A1-induced accumulation of MAP1LC3B-II during starvation in *MED1* KD cells (Figure 4C). Transcriptional induction of autophagy genes is necessary in order to sustain autophagy over prolonged periods of time. We thus examined the effects of *MED1* KD on

autophagy and lysosomal gene expression. As shown in Figure 4F, starvation induced the transcription of autophagosome and lysosome genes as well as several key TFs that regulate the transcription of autophagy and lysosomal genes in cells transfected with control siRNA. In contrast, the gene expressions of *MAP1LC3B, SQSTM1, ULK1, UVRAG* and *LAMP1* as well as the autophagy regulators *SESN2, FOXO1, FOXO3*, and *TFE3* were attenuated by *MED1* KD during starvation (Figure 4D).

We next examined colocalization of BODIPY and MAP1LC3B staining and found that there were more lipid-laden autophagosomes (yellow) in control hepatic cells than *MED1* KD cells in both glucose-replete and glucose-starvation conditions (Fig. S5). These findings showed that lipophagy of lipid droplets was impaired by the loss of *MED1* during both conditions. We then pre-loaded cells with or without fatty acids (0.1 mM palmitic acid and 0.2 mM oleic acid) overnight, and then subjected them to 24 h of glucose starvation. Cells then were stained for intracellular lipid using BODIPY fluorescent dye followed by flow cytometry measurement before and after 24 h of glucose starvation. We determined starvation-induced lipid oxidation by measuring the difference in BODIPY fluorescence before and after starvation. We observed significant decreases in lipid content after starvation in control cells regardless of whether fatty acids were loaded or not. In contrast, there were no decreases in starvation-induced lipid content in *MED1* KD cells during these conditions (Figure 5A). Since fatty acids are the primary fuel for hepatic cells during starvation, we next examined the effects of *MED1* KD on fatty acid-stimulated OCR using Seahorse extracellular flux analyzer. We found that basal respiration, ATP turnover, maximum respiratory capacity, and spare respiratory capacity were induced by fatty acids in control cells, but not in *MED1* KD cells (Figure 5B). mRNA levels of *PPARA* and *PPARGC1A*, which regulate fatty acid β-oxidation and mitochondrial biogenesis, also were significantly decreased in *MED1* KD cells during starvation (Figure 5C). Taken together, our results showed that loss of *MED1* led to decreased autophagic breakdown of lipid droplets and mitochondrial oxidation of fatty acids during starvation.

Induction of hepatic autophagy and β-oxidation by starvation is attenuated in *Med1* liver-specific KD (*Med1* LKD) mice.

We next investigated the role of *Med1* in the regulation of hepatic autophagy and β-oxidation during acute feeding *vs.* starvation *in vivo*. Ten-week old male C57BL/6 mice were injected with adeno-associated virus serotype-8 carrying *Med1* shRNA under the control of *Alb* promoter (AAV8-ALBp-eGFP-m*Med1*-shRNAmir) or control AAV8-Null to generate *Med1* liver-specific KD (*Med1* LKD) mice and control mice, respectively. Three weeks after injections, these mice were given normal chow diet from 9 am to 3 pm, or fasted for 22 h before sacrificing them and harvesting their livers. We demonstrated that hepatic *Med1* KD *in vivo* was successful by showing *Med1* mRNA and protein expression was decreased during fed and starvation states in the *Med1* LKD mice (Fig. S6A and Figure 6A). Furthermore, the mRNA
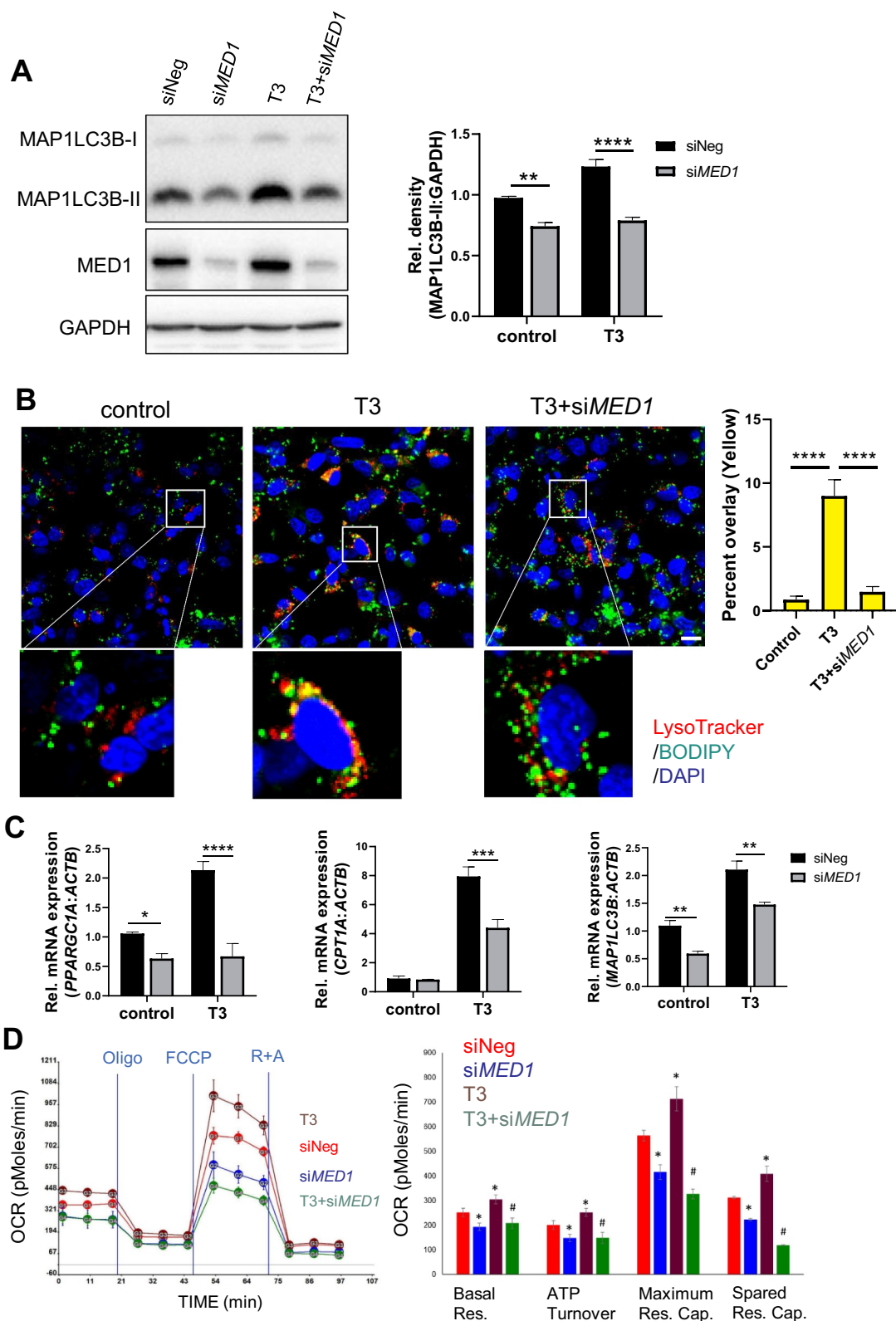
Figure 3. siRNA KD of *MED1* decreased T$_3$-induced lipophagy and mitochondrial activity in HepG2-TRβ cells. Forty-eight h after KD of *MED1*, the cells were treated with or without 100 nM T3 for another 24 h. (A) Immunoblot and densitometric analysis of MAP1LC3B-II showing that KD of *MED1* decreased T$_3$-induced autophagy. Data are represented as mean ± SEM (n = 3). (B) KD of *MED1* decreased T$_3$-induced lipophagy. Cells were stained with LysoTracker (200 nM, red) and BODIPY 493/503 (1 μg/mL, green). Colocalization of LysoTracker (lysosome) and BODIPY (lipid droplets) is shown as yellow spots. Scale bar: 20 μm. Percent colocalization of each cell was quantified. Data are represented as mean ± SEM (n = 25). (C) KD of *MED1* decreased T$_3$-induced transcription of *PPARGC1A, CPT1A and MAP1LC3B*. Data are represented as mean ± SEM (n = 3). (D) Seahorse XF Mito Stress Test showed that KD of *MED1* decreased T$_3$-induced mitochondrial activity. KD of *MED1* decreased basal respiration (Basal Res.), ATP turnover, maximum respiratory capacity (Maximum Res. Cap.), and spared respiratory capacity (Spared Res. Cap). Data are represented as mean ± SEM (n = 6).
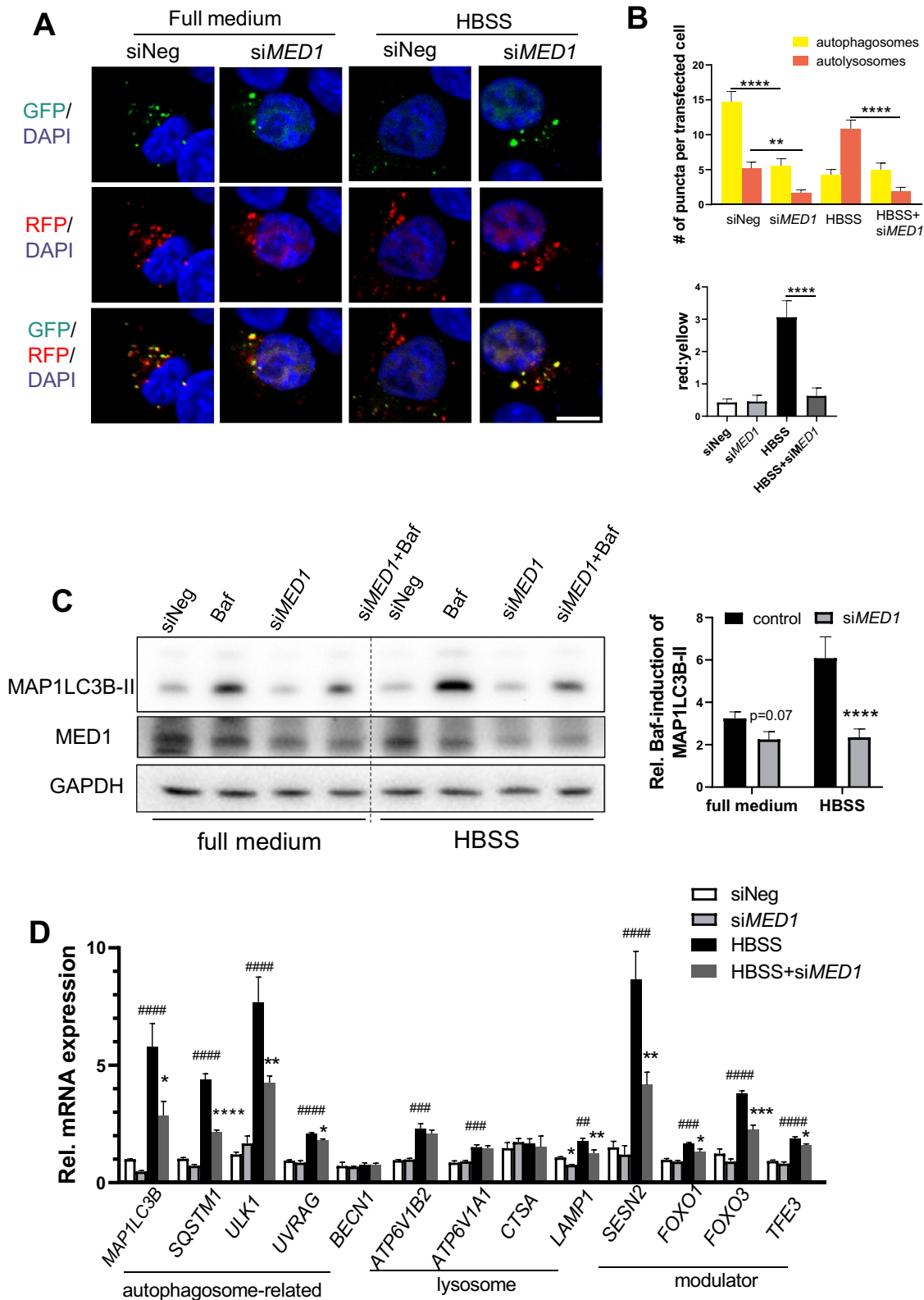
Figure 4. siRNA KD of *MED1* decreased starvation-induced autophagy. (A-B) Evaluation of autophagy flux using tandem RFP/GFP-tagged MAP1LC3B plasmid in HepG2 cells with or without 8 h HBSS starvation. Representative image (A) and Quantification (B) of autophagosomes (yellow puncta on overlay) and autolysosomes (RFP puncta on overlay) in tandem RFP/GFP-tagged LC3 plasmid transfected HepG2 cells with or without *MED1* KD. Yellow or red puncta per transfected cells were counted. Scale bar: 10 μm. Data are represented as mean ± SEM. (n ≥ 15). (C) Immunoblot and densitometric analysis showing Baf-caused accumulation of MAP1LC3B-II was decreased by KD of *MED1* under HBSS starvation. Forty-eight h after siRNA (10 nM) KD of *MED1*, cells were cultured in full medium or HBSS for 1 h. Baf (150 nM) was added 4 h before cells were harvested. Bars represent the mean of the respective individual ratios ± SEM (n = 3). (D) HBSS (8 h) starvation-induced expression of autophagic genes were impaired by *MED1* KD. Data are represented as mean ± SEM (n = 3).
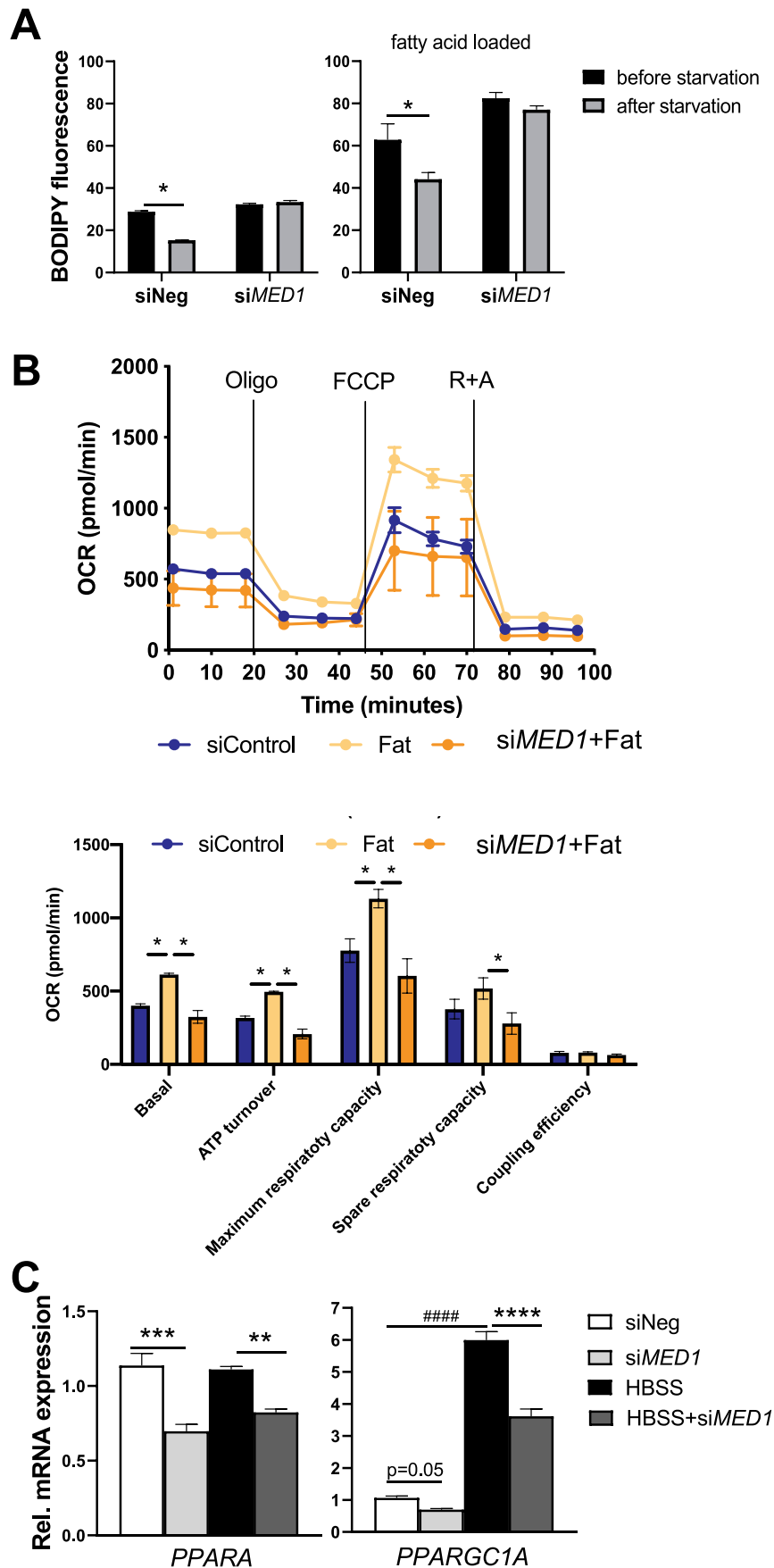
Figure 5. siRNA KD of *MED1* decreased oxidative phosphorylation, and lipid clearance in HepG2 cells. (A) KD of *MED1* decreased starvation-induced lipid oxidation. 48 h after transfection with control or *MED1* siRNA, HepG2 cells were loaded with or without 2% BSA-conjugated fatty acid (0.1 mM palmitic acid and 0.2 mM oleic acid) overnight. To Measure the lipid content before starvation, cells were stained with BODIPY (5 µg/ml) for 10 min, and harvested for flow cytometry measurement. To measure lipid content after starvation, the medium was replenished with 5% FBS containing, glucose and pyruvate-free medium for another 24 h. The cells then

were stained with BODIPY 493/503, and harvested for flow cytometry measurement. Thus, the difference in BODIPY fluorescence before and after starvation condition represented the starvation-induced lipid oxidation. Data are represented as mean ± SEM (n = 3). (B) Seahorse XF Mito Stress test showed that KD of *MED1* decreased fatty acids (Fat)-stimulated mitochondrial activity. Data are represented as mean ± SEM (n = 6). (C) HBSS (8 h) starvation-induced expression of metabolic genes were impaired by *MED1* KD. KD of *MED1* decreased key metabolic genes *PPARA* and *PPARGC1A*. Data are represented as mean ± SEM (n = 3).

levels of three TH target genes, *Dio1, Thrsp* and *Me1* were decreased in *Med1* LKD mice (Fig. S6B-D). Interestingly, T_3-treated mice showed an increase in *Med1* mRNA expression in a time-dependent manner (Fig. S7). Starvation did not change hepatic MAP1LC3B expression but decreased SQSTM1 protein expression in control mice (black bars) suggesting that there was increased autophagic degradation caused by starvation. In contrast, hepatic protein levels of MAP1LC3B-II was lower and SQSTM1 was higher in *Med1* LKD mice than in control mice during both the fed and starved states, indicating there was decreased autophagy in the *Med1* LKD mice during both conditions (Figure 6A). We next measured the level of β-hydroxybutyrate, the end product of β-oxidation. Starvation increased serum β-hydroxybutyrate levels in mice injected with control AAV8; however, this increase was attenuated in *Med1* LKD mice (Figure 6B). We next measured the hepatic and circulating triglyceride (TG) levels. Interestingly, there was an elevation of serum TG level, but no change in hepatic TG, in *Med1* LKD mice during both fed and fasting states (Figure 6C). Taken together with our previous findings in hepatic cells, these results showed that autophagy and β-oxidation of fatty acids induced by starvation was impaired by loss of *Med1 in vivo*. Transcriptional pathway analysis of the hepatic transcriptomes of control and *Med1* LKD mice during the fed and fasting states showed that several of the major gene pathways affected by *Med1* LKD during the fed and fasting states were involved in hormone signaling, fatty acid, glucose, ketone metabolism, and gluconeogenesis (Table 1, and Table S1).

Induction of hepatic genes involved in autophagy, lysosomal degradation, and lipid metabolism by starvation is attenuated in *Med1* LKD mice

Autophagy plays a prominent role in cellular fasting response, fatty acid metabolism, and ketogenesis. All of these pathways, including autophagy were decreased in *MED1* KD cells. We thus examined the hepatic expression of target genes involved in autophagy and lysosome function in *Med1* LKD mice. Three general patterns of gene expression emerged when genes involved in lysosome and autophagy function were analyzed. In one group, were increased by starvation in control mice and the increases were attenuated in *Med1* LKD mice (Figure 7). Genes such as *Map1lc3b, Vps113c, Atp6v0d2, Atp6v1b1, Sesn2*, and *Tfeb* displayed this gene expression pattern. In the second group, gene expression was not changed by fasting in control mice but was attenuated in both the fed and fasting states in *Med1* LKD mice. This pattern was observed in genes such as *Atg7, Vps13d, Ctsa, Lamp1*, and *Lamp2*. Yet another group exhibited increased gene expression after fasting, while the *Med1* LKD mice had decreased expression during both the fasting and fed states (*e.g., Ulk1, Foxo1*). These findings suggested that *Med1* regulated both basal and starvation-induced expression of some genes involved in

autophagy and lysosomal function whereas it selectively attenuated starvation-induced gene expression in others.

Induction of hepatic mitochondrial genes by starvation is attenuated in Med1 *LKD mice*

We earlier observed that *Med1* KD decreased oxidative phosphorylation in hepatic cells (Figure 2, Figure 3, and Figure 4). We thus examined the effects of *Med1* KD on the expression of genes involved in mitochondrial function or biogenesis during the fed and fasting states (Figure 8). *Ppargc1a* and *Ppara* mRNA expression was induced by starvation in control mice but this starvation-induced increase was attenuated in *Med1* LKD mice. mRNA expression of a mitochondrial protein (*Cox18*), mitochondrial enzymes (*Cs, Fh1*) and subunits belonging to mitochondrial electron transport chain (ETC) complexes (*Ndufb8, Sdhb, Uqcrc2, Atp5a1*) as well as a lipid metabolic enzyme (*Acsl1*) did not change between the fasting and fed states in control mice; however, the expression of most of these genes were reduced in both the fed and starvation states in *Med1* LKD mice.

Impaired PPARA – and FOXO1- mediated transcription in the livers of *Med1* LKD mice

In order to identify the NR or TF that might require *Med*1 for their transcription activity in the liver under starvation, we uploaded 252 hepatic genes that were downregulated in *Med1* LKD mice during fasting that were identified by RNA-seq analysis (235 genes) and qRT-PCR (17 genes), and performed ChIP Enrichment Analysis [26] (ChEA-2016, https://maayanlab.cloud/Enrichr/). This program employs transcription factor binding site profiles from published CHIP-chip and CHIP-seq studies. Interestingly, the downregulated hepatic genes in the *Med1* KD mice during fasting were enriched for genes containing NR or TF binding sites (Table S2). Previous studies showed that RXR, LXR, PPARA, ESR1, and thyroid hormone receptors were NRs that required MED1 for their transcription activity [27–29]. Transcriptionally-regulated genes containing their binding sites (NRs: *Ppara, Esr1, Lxr, and Rxr*, and transcription factors: *Egr1, Nfe2, and Foxo1*) were identified by this unbiased approach. Notably, *Ppara, Esr1, Egr1, Nfe2*, and *Foxo1* regulate autophagy at the transcriptional level [15,30–33]. In particular, both *Ppara* and *Foxo1* have been reported to regulate hepatic autophagy and energy homeostasis (e.g., lipid oxidation or gluconeogenesis) during starvation. We found the mRNA and protein expression of *Ppara* and *Foxo1* were decreased in the livers of *Med1* LKD animals (Fig. 8, Fig. 9A). We also used qRT-PCR to validate additional putative PPARA and FOXO1 target genes *Kcnk5, Tat, Insig2, Pdk1, Igfbp1, G6pc, Abca8a, Pck1, Lpin1, Ahcy*, and *Klf9*. Most of these genes are highly involved in lipid or glucose metabolism, and all of them were downregulated at the mRNA level in *Med1* LKD mice (Figure 9B). Additionally, the mRNA expression of several autophagic and mitochondrial genes that are putative target genes of *Ppara* including *Map1lc3b, Atp6v0d2*,
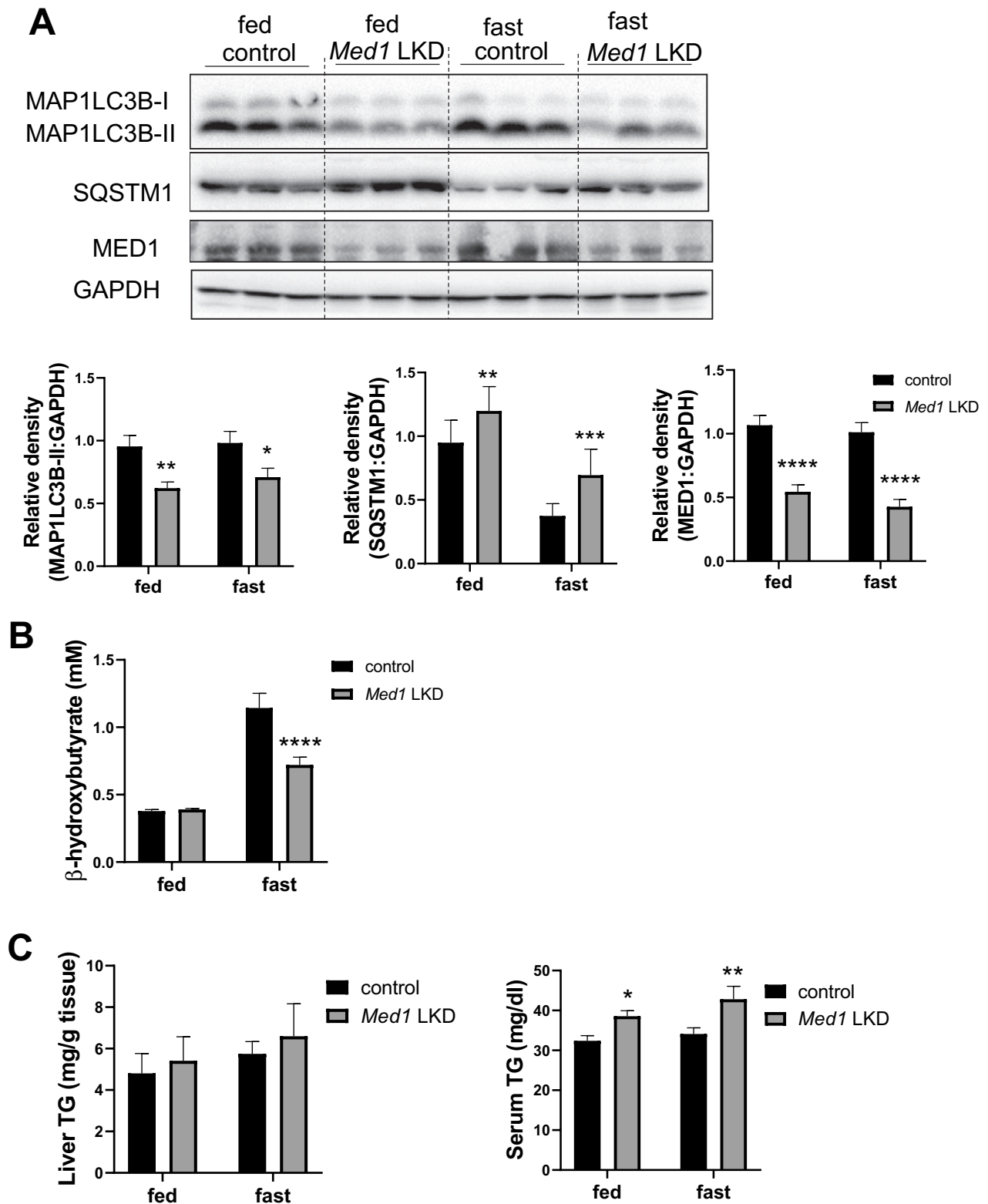
Figure 6. Liver-specific KD of *Med1* decreased autophagy and fatty acid β-oxidation *in vivo*. Liver-specific KD of *Med1* or control animals were generated by injecting ALB-m*Med1*-shRNA-expression adeno-associated virus (AAV8-ALBp-eGFP-m*Med1*-shRNAmir) or control adenovirus. (A) Immunoblot and densitometric analysis of MAP1LC3B-II, SQSTM1 in the liver from control or *Med1* KD C57BL/6 J mice under fed or fasting condition. (B) Serum β-hydroxybutyrate and (C) Hepatic TG, serum TG levels from control or *Med1* KD C57BL/6 J mice under fed or fasting condition. Data are represented as mean ± SEM. Control fed (n = 7), si*Med1* LKD fed (n = 8), fast control (n = 8), si*Med1* LKD fast (n = 8).

Table 1. Gene Set Enrichment Analysis (GSEA) pathway analysis of transcriptomics performed in the livers from fed or fasting mice with control or *Med1* shRNA under the *Alb* promoter carried by AAV8.

	Corrected P value	
GO Pathway description	fed+Med1 LKD vs. fed	fast+Med1 LKD vs. fast
GO:0009725_response to hormone	3.43E-15	2.02E-08
GO:0006631_fatty acid metabolic process	2.62E-13	7.11E-07
GO:0006805_xenobiotic metabolic process	6.17E-11	0.003916
GO:0043434_response to peptide hormone	4.39E-10	2.13E-09
GO:0042738_exogenous drug catabolic process	5.18E-10	0.40569
GO:0010906_regulation of glucose metabolic process	1.94E-09	1.26E-08
GO:0006111_regulation of gluconeogenesis	1.62E-08	0.000101
GO:0042180_cellular ketone metabolic process	5.24E-08	0.000247

Fh1, and *Cs* were downregulated in livers from *Med1* LKD mice (Table S2). Taken together, our data showed that knockdown of *Med1* in the liver decreased both mRNA and protein levels of *Foxo1*, and *Ppara*, and the mRNA expression of their target genes. These results suggested that during fating, *Ppara*- and *Foxo1*-mediated transcription likely were impaired in the livers of *Med1* LKD animals.

Basal expression of hepatic Med1 protein as well as autophagy is reduced in mouse models of nonalcoholic fatty liver disease (NAFLD)

We next examined whether there was a decrease in hepatic *Med1* expression in NAFLD by employing two mouse models of NAFLD [34]. Mice that were fed Western Diet with 15% fructose in drinking water (WDF) for 16 weeks had increased liver triglyceride content (Figure 10A). We also found they had decreased *Med1* protein expression (Figure 10B). There also was no change in MAP1LC3B-II in the livers from mice fed WDF; however, there was accumulation of SQSTM1 in these mice (Figure 10B-C), suggesting that there was decreased autophagy in NAFLD when *Med1* expression was decreased. A genetic model of NAFLD, *Lepr*db/db mice (db/db), can develop hepatosteatosis when fed normal chow diet in an age-dependent manner [34]. We analyzed the livers from 12 weeks old C57BL/6 J wildtype and db/db mice fed normal chow diet *ad libitum*, and found that db/db mice showed increased hepatic triglyceride content (Figure 10D), decreased protein level of MED11, and increased accumulation of both MAP1LC3B-II and SQSTM1 (Figure 10E-F). Taken together, the two models of NAFLD displayed hepatosteatosis and impaired autophagy that was associated with decreased level of *Med1* protein expression. These findings raise the possibility that changes in *Med1* could contribute to the decreased autophagy and hepatic lipid metabolism that occur in NAFLD.

Discussion

Recent evidence has shown that transcriptional regulation of autophagy is important for maintaining basal autophagy and regenerating autophagy/lysosome components degraded during chronic conditions such as prolonged starvation [8–11,35]. TFs such as CREB [16], TFEB [36], FOXO1 [37], and PPARA [15] play key roles in the induction of autophagy gene transcription during starvation; however, little is known about the role of their transcriptional co-activators. In the current study, we have provided several lines of evidence suggesting that the co-activator, *MED1* is involved in regulating hepatic autophagy during both fed and starved conditions (Fig. 1, Fig. 4, Fig. 6), and after T_3 treatment (Figure 3). In cultured hepatic cells and in mice with liver-specific KD of *Med1*, we observed transcription of hepatic genes under both nutrient replete/fed and fasting conditions (Fig. 2A, Fig. 4D, and Fig. 7). The genes included proteins involved in autophagosome and lysosome formation, tethering proteins, autophagy receptors, and transcriptional modulators. These genes were upregulated during starvation. However, after *Med1* KD, the expression of some of these genes attenuated during fasting conditions, whereas others were attenuated during both conditions.

During starvation, autophagy is activated to break down macromolecules that provide substrates for gluconeogenesis and fatty acids for mitochondrial metabolism [6,38]. The decreased supply of nutrients and/or lower energy stores within the cell, leads to increased hepatic lipophagy [6]. In this connection, we observed increased autophagy and decreased amounts of intracellular lipid in hepatic cells during starvation, which were attenuated in *MED1* KD cells (Fig. 4, Fig. 5A). The number of lipophagosomes were also decreased in *MED1* KD cells (Fig. S5). Furthermore, the increases in starvation-induced autophagy and serum β-hydroxybutyrate observed in control mice were not found in the *Med1* LKD mice (Figure 6B). Taken together, our data strongly suggest that *MED1* KD in hepatic cells led to decreased autophagy and decreased fatty acid β-oxidation during starvation.

We also investigated the role of *MED1* on mitochondrial activity and oxidative phosphorylation by using Seahorse XF extracellular flux analyzer to perform cell energy phenotype, mitochondrial stress, and mitochondrial fatty acid oxidation tests. *MED1* KD decreased mitochondrial OCR with little effect on anaerobic glycolysis, mitigated OCR during mitostress conditions, attenuated OCR response to long chain fatty acid supplementation, and reduced lipid clearance (Figure 2C-F, Figure 5A-B). We also found that *MED1* KD resulted in decreased transcription of mitochondrial genes in both cultured hepatic cells as well as in mouse liver (Fig. 2B, Fig. 5C, and Fig. 8). In the livers of *Med1* LKD mice, genes encoding enzymes in ETC complexes, enzymes involved in oxidative phosphorylation, and key regulators for mitochondrial biogenesis such as *Ppargc1a and Ppara* were downregulated (Figure 8). Additionally, loss of *Med1* decreased lipid oxidation during starvation through reduced transcription of autophagy, lysosomal, and mitochondrial genes (Fig. 7–8). RNA-seq and pathway analysis showed that genes regulated by *Med1* belonged to pathways involved in hormone response as well as fatty acid and glucose metabolism (Table 1 and Table S1).

Increased lipophagy, mitochondrial oxidative phosphorylation capacity, and β-oxidation of fatty acids have been reported for NRs such as PPARA and TR [6,7,25,39,40]. Interestingly, both PPARA and TR directly bind to *MED1*,
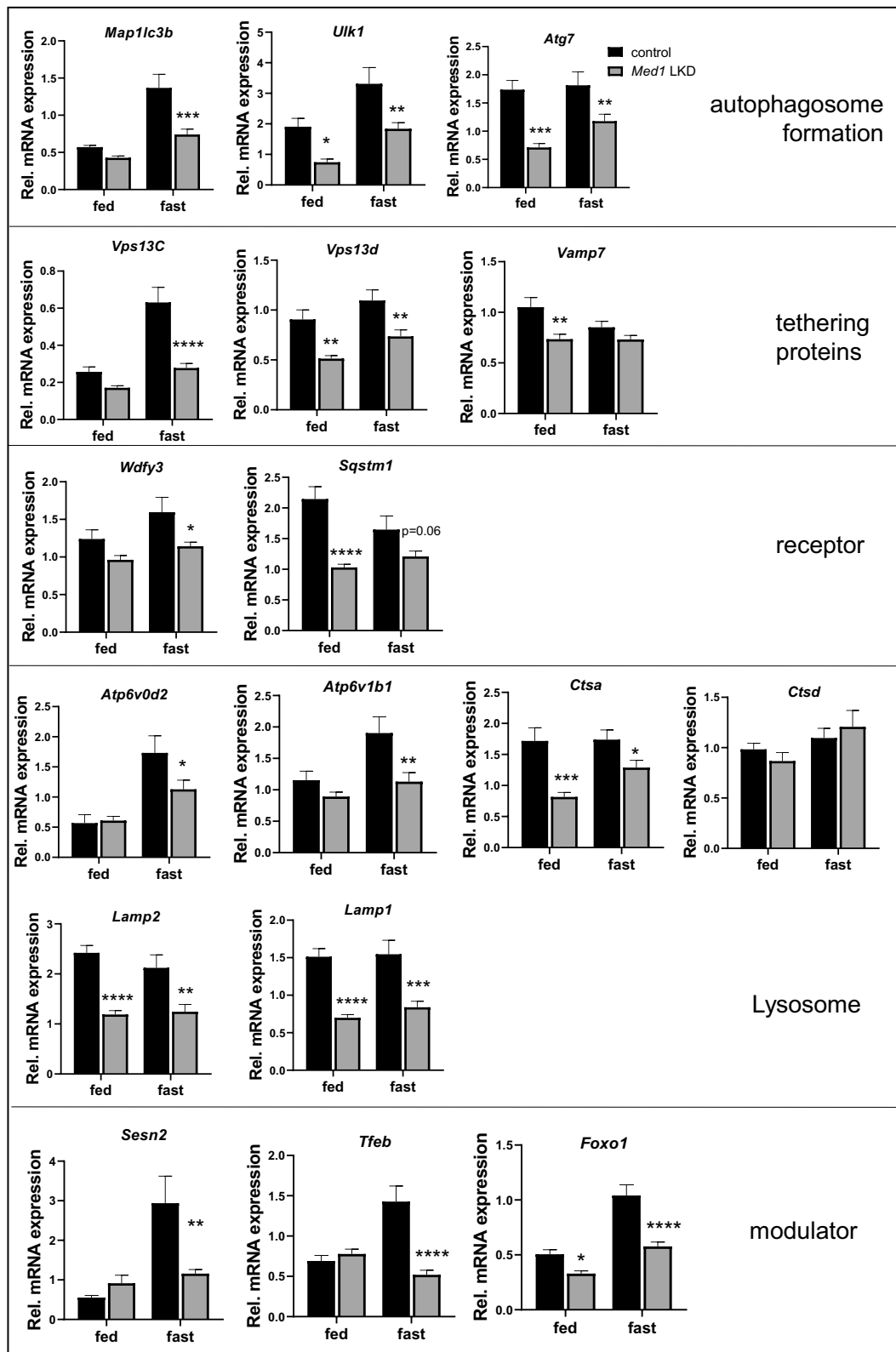
Figure 7. Expression of autophagy genes was attenuated in the livers from control or *Med1* LKD mice under fed or fasting conditions. Data are represented as mean ± SEM. Control fed (n = 7), si*Med1* LKD fed (n = 8), fast control (n = 8), si*Med1* LKD fast (n = 8).

which serves as a co-activator for their ligand-mediated transcription [20,27,41]. We found that *MED1* played a key role in TR-mediated transcriptional activity since the induction of several target genes by T_3 in control hepatic cells was dampened in *MED1* KD cells (Figure 3C). Significantly, the increases in autophagy, lipophagy,
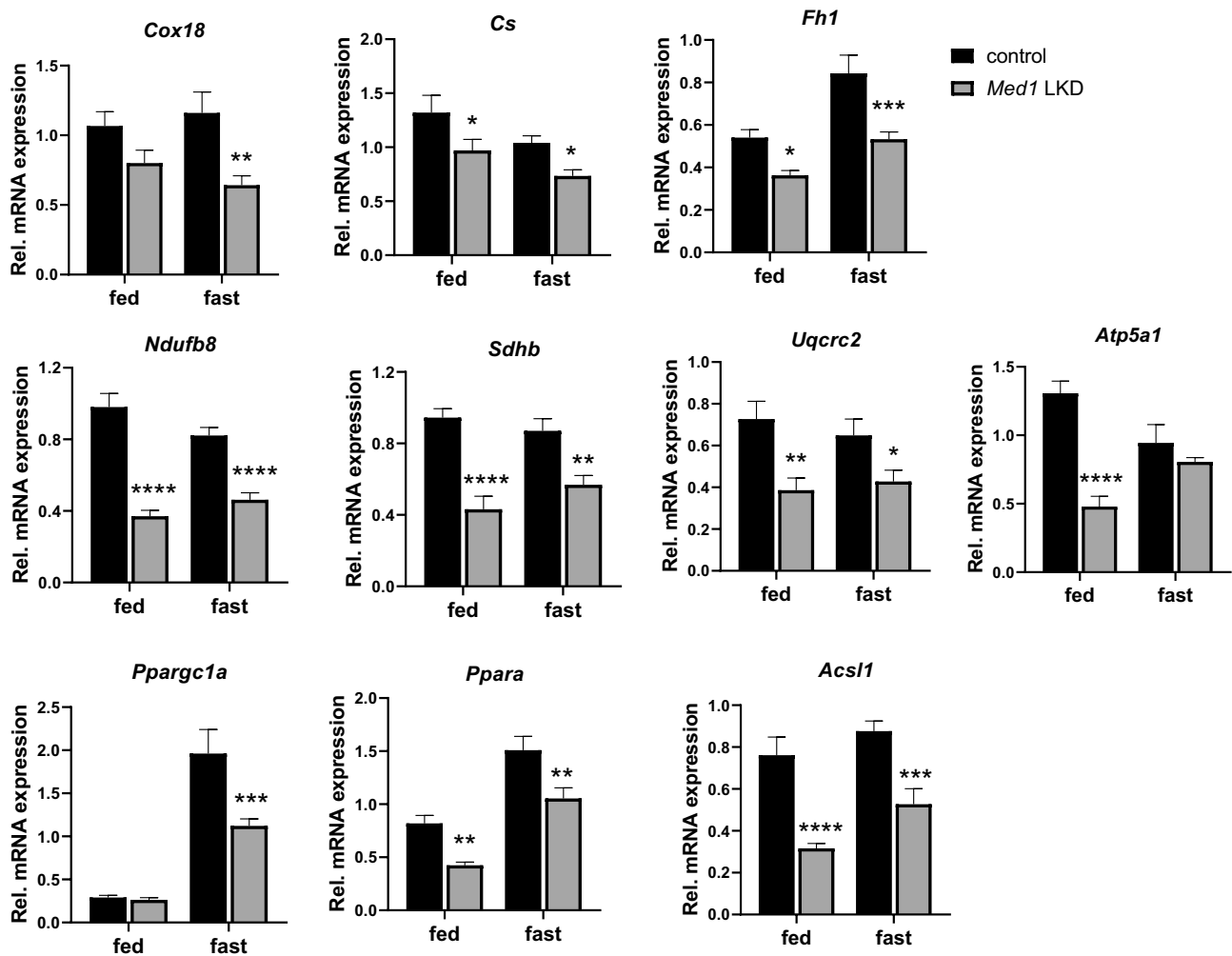
Figure 8. Expression of mitochondrial and metabolic genes was attenuated in the livers from control or *Med1* LKD mice under fed or fasting conditions. Data are represented as mean ± SEM. Control fed (n = 7), si*Med1* LKD fed (n = 8), fast control (n = 8), si*Med1* LKD fast (n = 8).

oxygen consumption and ATP production by T_3 observed in control hepatic cells also were decreased in *MED1* KD cells (Figure 3). Thus, these findings demonstrate a critical role of *MED1* on T_3-mediated effects on these processes. Interestingly, we also found that long-term T_3 treatment of mice induced the expression of hepatic *Med1* mRNA (Fig. S6). This raises the intriguing possibility that concurrent rises in T_3 and *Med1* co-activator levels could synergistically increase the sensitivity and response of target genes to TH. In this connection, we observed the gene expressions of *Thrsp* and *Me1*, two well-known TH-regulated target genes, were decreased in the *Med1* LKD mice during both the fed and fasting states (Fig. S6).

To understand the global effects of *Med1* on transcription during starvation, we performed RNA-seq and qRT-PCR analysis in the livers from control and *Med1* LKD animals under fed and fasting conditions, and identified the downregulated genes due to KD of *Med1*. Some of these genes were involved in autophagy, mitochondrial function, as well as lipid and glucose metabolism (Fig. 7–8, Table S1). We then performed ChIP Enrichment Analysis (ChEA-2016) on this set of *Med1* target genes. PPARA and FOXO1, as well as RXR and LXR, were identified by this unbiased approach, suggesting that these NRs and TFs were

potential transcription factors regulating these genes through *Med1* (Table S2). Additionally, we found that hepatic mRNA levels of *Ppara* and *Foxo1* target genes were decreased during starvation in *Med1* LKD mice (Figure 9B and Table S2). Furthermore, the hepatic mRNA and protein expression of *Ppara* and *Foxo1* were decreased in *Med1* LKD mice (Figs. 8 and Fig. 9A), suggesting yet another mechanism for regulating their activities. In this connection, it is noteworthy that previous studies showed that KD of *Med1* inhibited ESR1-induced *Foxo1* transcription [29], whereas PPARA directly bound to *Med1*'s LxxLL motif and utilized *Med1* as an indispensable co-activator for its transcriptional activity [27,42]. Our findings suggest that during starvation, *MED1* may be involved in the induction of autophagy genes regulated by PPARA, FOXO1, and other transcription factors.

Finally, we found reduced *Med1* expression in two mouse models of NAFLD: mice fed WFD for 16 weeks and *Lepr*[db/db] (db/db) mice. Additionally, there was decreased hepatic autophagy and increased hepatosteatosis in both NAFLD mouse models. These findings suggest that reduced hepatic *MED1* expression in NAFLD may be involved in the decreased hepatic autophagy, mitochondrial function, and β-oxidation found in this condition.
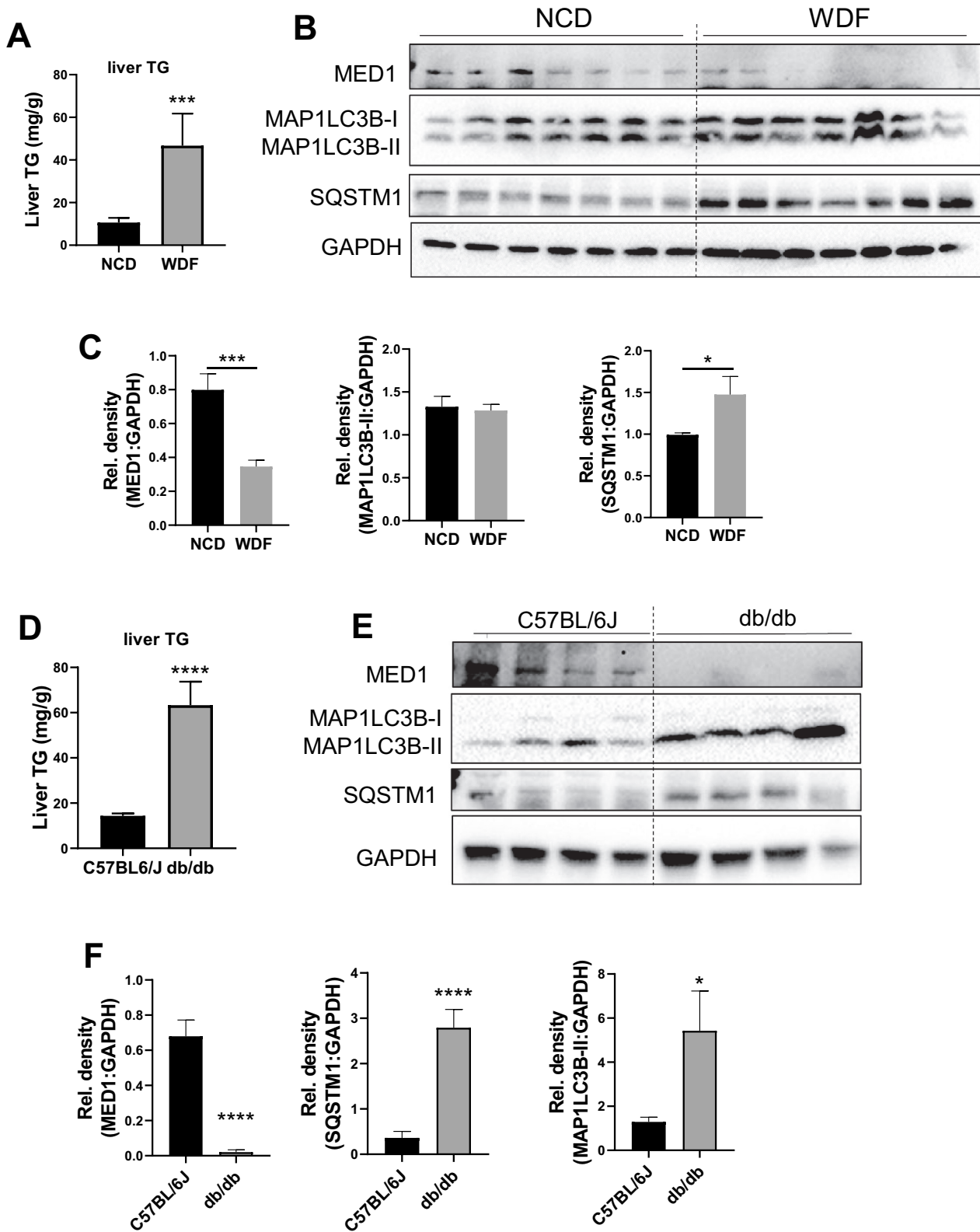
Figure 9. PPARA and FOXO1 protein levels, and mRNA expression of their target genes in the livers from control or *Med1* LKD mice under fed or fasting conditions. (A) Immunoblot and densitometric analysis of PPARA, and FOXO1 in the liver from control or *Med1* KD C57BL/6 J mice under fed or fasting condition. (B) Quantitative RT-PCR measurement of *PPARA* and *FOXO1* target genes. Data are represented as mean ± SEM. Control fed (n = 7), si*Med1* LKD fed (n = 8), fast control (n = 8), si*Med1* LKD fast (n = 8).

Figure 10. *Med1* protein and autophagy was decreased in animal models of hepatosteatosis. (A-C) *Med1* protein level was decreased in WDF feeding-induced hepatosteatosis. Liver triglyceride content was measured in the liver from C57BL/6 J mice fed with NCD (n = 5) or WDF (n = 5) diet for 16 weeks (A), Immunoblot (B), and densitometric analysis (C) of *Med1*, MAP1LC3B-II, and SQSTM1 in the liver from C57BL/6 J mice fed with NCD (n = 7) or WDF (n = 7) diet for 16 weeks. (C-F) A lower protein level of *Med1* was observed in the liver from db/db mice than age-matched C57BL/6 J mice. Liver triglyceride content was measured in the liver C57BL/6 J (n = 5) or db/db (n = 5) mice fed with NCD diet (D), Immunoblot (E), and densitometric analysis (F) of *Med1*, MAP1LC3B-II, and SQSTM1 in the liver from C57BL/6J (n = 8) or db/db (n = 8) mice fed with NCD diet. Data are represented as mean ± SEM.

In summary, we have demonstrated that *MED1* mediator subunit plays an important role in the regulation of autophagy during fed and starvation states. Our findings suggest that *MED1* regulation of autophagy may be a novel mechanism to control autophagy, β-oxidation, oxidative phosphorylation, and lipid metabolism. Declines in hepatic *MED1* level in NAFLD may contribute to the pathogenesis of this condition. Additionally, pathway analysis of the control and *Med1* LKD mice transcriptomes showed that *Med1* serves as modulator of a wide range of cellular metabolic programs and pathways. Thus, *MED1* most likely integrates the signaling of multiple TFs and NRs that utilize it as a co-activator, and its expression also may augment or dampen the transcriptional activity by TFs and NRs, particularly during different nutrient or hormonal states. Our findings demonstrate not only the important role of *MED1* and Mediator complex for the transcriptional activity of NRs but also demonstrate that it is a key participant in promoting autophagy and metabolic homeostasis in the liver during different nutrient and hormonal conditions.

Materials and Methods

Reagents

Antibodies recognizing MAP1LC3B/LC3B (2775), GAPDH (2118), SQSTM1/p62 (5114) were purchased from Cell Signaling Technology, antibody recognizing *MED1* was purchased from Bethyl Laboratories (A300-793A), whereas antibodies recognizing ACTB/β-actin (sc-47,778), and HRP-conjugated secondary antibodies recognizing mouse (sc-2005) and rabbit (sc-2357) IgG were purchased from Santa Cruz Biotechnology. Control or *MED1* siRNA targeting human or mouse *MED1* were purchased from Dharmacon (L-004126-00-0005). Culture media (D5796) from Invitrogen, and serum (F2442) from Sigma-Aldrich. GFP-RFP-LC3 (tf-LC3) (Addgene, 21,074) and eGFP-LC3 (Addgene, 21,073) plasmids were gifts from Prof. T. Yoshimori (Osaka University, Osaka, Japan) [24,43].

Cell Culture and Transfection

HepG2 cells were purchased from ATCC (HB-8065) and maintained at 37°C in DMEM containing 10% FBS in a 5% CO_2 atmosphere. For siRNA transfection, HepG2, HepG2-TRβ, or AML12 cells were trypsinized, mixed with opti-MEM medium (Invitrogen, 31,985,070) containing Lipofectamine RNAimax (Invitrogen, 13,778,150) and *MED1* or control siRNA (10 nM) according to the manufacturer's recommendations. For cDNA transfection, GFP-RFP-LC3 (tf-LC3) and eGFP-LC3 plasmid was transfected into HepG2 cells using Lipofectamine 2000 reagent (Invitrogen, 11,668,019) 48 h after the transfection of control or *MED1* siRNA.

For nutrient-deprived conditions, amino acid deprivation was introduced by replenish the normal nutritional medium with HBSS (Gibco, 14,025–092); glucose deprivation was introduced by replenishing the medium with DMEM (without glucose, sodium pyruvate; Mediatech Inc, 17–207-cv) containing 5% FBS, which was referred to as starvation.

To assess the effect of *MED1* KD under basal condition, HepG2 cells were transfected with negative control or *MED1* siRNA. Cells were harvested 48 h after transfection.

To assess the effect of *MED1* KD on T_3 action, HepG2-TRβ cells were transfected with negative control or *MED1* siRNA. 48 h after transfection, cells were treated with or without 100 nM T_3 (Sigma-Aldrich, T6397) for another 24 h.

Crystal violet staining

Forty-eight h after transfection with control or *MED1* siRNA, HepG2 cells were washed with PBS (VWR Life Science, VWRCE504-500ML), fixed with 90% ethanol and stained with 0.1% crystal violet. Following extensive washing with tap water and air-dry, dye was extracted with 10% acetic acid and quantified by measuring absorbance at 595 nm on a multiwall spectrophotometer (Bio-Rad).

Western blot analysis

Proteins were separated by SDS–PAGE under reducing conditions and transferred to nitrocellulose membranes. Membranes were blocked with 5% nonfat milk in phosphate-buffered saline with 0.1% Tween 20 (Sigma-Aldrich, P9416; PBST). The blots were incubated overnight at 4°C with primary antibodies. Immunoblot analysis was performed using an enhanced chemiluminescence procedure (GE Healthcare, RPN2106).

For autophagy flux analysis, the bafilomycin A_1 (150 nM for HepG2 cells, and 10 nM for AML12 cells; ATCC, CRL-2254) was added 4 h before cells were harvested.

Immunofluorescence studies

For endogenous MAP1LC3B puncta staining, cells were washed in PBS and then fixed with 4% paraformaldehyde for 15 min at room temperature. Fixed cells were washed with PBS, permeabilized in 100% methanol for 10 min at – 20°C, washed in PBS, and blocked in blocking buffer for 1 h at room temperature. Cells subsequently were incubated with anti- MAP1LC3B antibody (1:300 dilution) overnight at 4°C. After 3 TBST washes, cells were incubated with Alexa Fluor–anti-rabbit antibody (Invitrogen, A27034) for 2 h at room temperature and then washed 3 times in TBST. Coverslips were mounted on slides using Vectashield anti-fade reagent with 4′,6-diamidino-2-phenylindole (Invitrogen, P36931). Cells were visualized using LSM710 Carl Zeiss confocal microscope.

To assess the effect of *MED1* KD on T_3-induced lipophagy, 48 h after HepG2-TRβ cells were transfected with negative control or *MED1* siRNA, cells were treated with 100 nM T_3 for 24 h. Cells were stained with LysoTracker Red DND-99 (Thermo Fisher Scientific, L7528; 200 nM) for 60 min, washed with PBS, fixed with 4% formaldehyde. Fixed cells was stained with BODIPY 493/503 (1 μg/ml; Invitrogen, D3922) and DAPI (Invitrogen, D1306). Colocalization of LysoTracker and BODIPY was performed using CoLocalizer Pro software (CoLocalization Research Software).

To assess the effect of *MED1* KD on starvation-induced lipophagy, 48 h after HepG2 cells were transfected with negative control or *MED1* siRNA, the cells were loaded with BSA-

conjugated fatty acids (0.1 mM palmitic acid [Sigma-Aldrich, P0500], 0.2 mM oleic acid [Sigma-Aldrich, O1008]); overnight. To starve the cells, the medium was replenished with 5% FBS containing glucose and pyruvate-free medium. Cells were cultured for another 24 h before fixation. Colocalization analysis of MAP1LC3B and BODIPY was performed using CoLocalizer Pro software.

Cellular oxygen consumption rate (OCR) analysis

Mitochondrial stress test was performed using Mito stress test kit (Seahorse Biosciences, 103,015–100). Oxygen consumption was measured at 37°C using an XF24 extracellular analyzer (Seahorse Bioscience Inc., North Billerica, MA, USA). HepG2 or HepG2-TRβ cells (40,000) were seeded in 24-well plates and transfected with *MED1* siRNA or negative control siRNA. Forty-eight h after transfection, mitochondrial metabolic parameters were assessed using Mito stress test kit according to manufacturer's instructions. Every point represents an average from five different wells. For T_3 treatment, 48 h after transfection with negative or *MED1* siRNA, HepG2-TRβ cells were treated with or without 100 nM T_3. For fatty acids loading, 48 h after transfection with negative or *MED1* siRNA, HepG2 cells were treated with 2% BSA-conjugated fatty acid (0.33 mM palmitic acid and 0.66 mM oleic acid) for 24 h.

Bioenergetic phenotyping and fatty acid oxidation assay were performed using Agilent Seahorse XFe96 Extracellular Flux Analyzer. Briefly, HepG2 cells (6,400) were seeded in 96-well plates transfected with negative or *MED1* siRNA. Forty-eight h after transfection, bioenergetic phenotyping or fatty acid oxidation assay was performed using XF Cell Energy Phenotype Test Kit or using long chain fatty acid oxidation inhibitor etomoxir (4 μM).

BODIPY 493/503 Staining and cellular fat content measurement in vitro

The neutral lipid was stained with fluorescent dye BODIPY 493/503 (5 μg/ml) for 10 min, followed by measurement using a Macsquant flow cytometer (Miltenyi Biotec) as previously described [44]. For measurement of neutral lipid under basal condition, 48 h after HepG2 cells were transfected with negative control or *MED1* siRNA, cells were stained with BODIPY 493/503 for measurement.

For fatty acid oxidation before and after starvation, 48 h after transfection with negative control or *MED1* siRNA, HepG2 cells were loaded with or without 2% BSA-conjugated fatty acid (0.1 mM palmitic acid and 0.2 mM oleic acid) overnight. For non-starved condition, the cells were stained and harvested for flow cytometry measurement. For the starved cells, the medium was replenished with 5% FBS containing glucose and pyruvate-free medium for another 24 h. Then the cells were stained with BODIPY 493/503, and harvested for flow cytometry measurement.

RNA purification and RT-PCR

Total cellular RNA was isolated with the High Pure RNA isolation Kit (Roche, 11,828,665,001) following the manufacturer's protocol and total RNA was quantified with a Nanodrop ND-1000 spectrophotometer. Total RNA (1 μg) was reverse-transcribed using iSCRIPT cDNA synthesis kit (Bio-Rad, 1,708,890) under conditions defined by the supplier. cDNA was quantified by real-time PCR on the Rotor-Gene Q System (Qiagen). PCR was done using QuantiFast SYBR Green PCR Kit (Qiagen, 204,156) according to the manufacturer's instructions.

For HBSS starvation, HepG2 cells were transfected with negative control or *MED1* siRNA. 48 h after transfection, the medium was replenished with full DMEM medium or HBSS for 8 h before RNA extraction.

Generation of liver-specific *Med1* KD mice

Animal studies were conducted in accordance with the principles and procedures outlined in the National Institutes of Health Guide for the Care and Use of Laboratory Animals and were approved by the Institutional Animal Care and Use Committee (IACUC) at the Duke-National University of Singapore Graduate Medical School. The authors confirm that all experiments were performed in accordance with relevant guidelines and regulations. The authors also confirm that the experimental protocol was approved by Duke-NUS Medical School, Singapore institutional committee.

Male C57BL/6 mice (8 weeks old) were obtained from NUSCARE and housed in hanging polycarbonate cages under a 12-h light/12-h dark cycle at 23°C with normal chow diet (Research Diests, D11112201) and water available ad libitum. Mice (10 weeks old) were injected with *Med1* shRNA carried by the *Alb* (albumin) promoter (*Albp*)-eGFP-expression adeno-associated virus (AAV8-*Albp*-eGFP-mMED1-shRNAmir) or control adeno-associated virus (AAV8-ALBp-eGFP-null). 1×10^{12} GC/mice in 0.25 ml of sterile 0.9% NaCl was injected through the tail vein. Four weeks after the injection, the mice were used for acute fasting and feeding experiment.

Acute fasting and feeding

Feeding after a fast was carried out as described [45]. Briefly, normal chow diet and cage bedding were removed at 5 PM until 10 AM the next day, and food was provided until 5 PM and removed again afterward. At 9 AM the next day, food was provided for 7 control AAV8 injected mice (fed control) and 8 *Med1* shRNA injected mice (fed *Med1* LKD) only, and other 8 control AAV8 injected mice (fast control) and 8 *Med1* shRNA-injected mice (fast *Med1* LKD) remained fasted. Six h later, animals were sacrificed in CO_2 chambers, blood and livers were collected. Liver tissue was snap frozen in liquid N_2 and subsequently used for protein and RNA isolation.

RNA-seq, pathway and ChIP Enrichment Analysis analysis

RNA was isolated from liver tissue using QIAzol (Qiagen, 79,306), followed by clean-up using Invitek Mini Kit (Invitek, 1,032,100,300) following the manufacturer's protocol. RNA-seq and pathway analysis on pooled samples of each

fed (n = 4), fed *with Med1* LKD (n = 4), fast, and fast with *Med1* LKD (n = 4) were performed by NovogeneAIT Genomics Singapore Pte Ltd. Briefly, Alignments were parsed using Tophat program and differential expressions were determined through DESeq2/edgeR. GO enrichment were implemented by the ClusterProfiler.

The downregulated genes (fast with *Med1* LKD *vs* fast) identified by RNA-seq analysis (235 genes), and qRT-PCR (17 genes) were used for ChIP Enrichment Analysis (ChEA-2016, https://maayanlab.cloud/Enrichr/) [26], which consists transcription factor binding sites profiles from published CHIP-chip, and CHIP-seq studies. Thus, this unbiased approach enabled us to identify putative NRs or TFs that requires *Med1* for its transcription under starvation.

Dietary and genetic models of hepatosteatosis

Previously characterized diet-induced NAFLD mice using WDF (western diet [Research Diets, D12079B] with 15% fructose [Sigma-Aldrich, 57–48-7] in the drinking water) feeding was used [34]. Male C57BL/6 J (10 weeks) were fed with normal chow diet (NCD) or WDF for 16 weeks before the animals were sacrificed, and livers were harvested.

Genetic mice model of NAFLD *Lepr*db/db (db/db) mice were purchased from The Jackson Laboratory (009659). Wild-type C57BL/6 J mice were obtained from NUSCARE (C57BL/6 JInv). Both db/db and C57BL/6 J were fed on NCD for 12 weeks, and sacrificed for tissue harvest.

Biochemical assays

Serum β-hydroxybutyrate and serum triglyceride content were determined using Cayman β-Hydroxybutyrate (Ketone Body) Colorimetric Assay Kit (700,190) and Triglyceride Colorimetric Assay Kit (10,010,303), respectively, according to manufacturer's instructions. Hepatic lipid from the control and *Med1* LKD mice under fed and fast was extracted as follows. 50 mg of liver tissue was homogenized in chloroform:methanol (2:1) mix (20 μl solution per 1 mg tissue) at 4000 rpm for 99 s. 500 μl tissue homogenate was transferred to a 1.5-ml tube, 500 μl of NaCl 0.9% and 500 μl chloroform were added, and vigorously shaken (2000 rpm) for 1 h at 4°C. Centrifuge at 18,800 g for 5 min at room temperature. Two phases will form, with an interphase in the middle. Part of the lower phase (500 μl; lipids and chloroform) was transferred to a new 1.5-ml tube. The solvent was removed by passing nitrogen gas in a in a fume hood. The lipid pellets were dissolved in 50 μl of 2% NP-40 (Sigma-Aldrich, 127,087–87-0) with sonication at amplitude 80 for 5 min. The extracted hepatic lipid samples were used to determine hepatic TG using Cayman Triglyceride Colorimetric Assay kit.

Statistics

Statistical analysis was performed using GraphPad Prism 8. For two experimental groups, statistical significance was determined by Student's t-test. For three experimental groups, One-way ANOVA was performed followed by Fisher's Least Significant Difference (LSD) test. For in vivo studies involve fed and fasted animals with or without liver-specific *Med1* KD, statistical significance was determined by two-way ANOVA analysis of variance followed Fisher's LSD multiple comparisons test.

Disclosure statement

The authors have no conflict of interest.

ORCID

Eveline Bruinstroop 🆔 http://orcid.org/0000-0001-6466-8497
Kenji Ohba 🆔 http://orcid.org/0000-0001-8538-8742

References

[1] Kaur J, Debnath J. Autophagy at the crossroads of catabolism and anabolism. Nat Rev Mol Cell Biol. 2015 Aug;16(8):461–472.
[2] Galluzzi L, Green DR. Autophagy-independent functions of the autophagy machinery. Cell. 2019Jun13; 177(7):1682–1699.
[3] Abdrakhmanov A, Gogvadze V, Zhivotovsky B. To eat or to die: deciphering selective forms of autophagy. Trends Biochem Sci. 2020 Apr;45(4):347–364.
[4] Eaton S. Control of mitochondrial beta-oxidation flux. Prog Lipid Res. 2002 May;41(3):197–239.
[5] Condello M, Pellegrini E, Caraglia M, et al. Targeting autophagy to overcome human diseases. Int J Mol Sci. 2019Feb8 20;(3)3.
[6] Singh R, Kaushik S, Wang Y, et al. Autophagy regulates lipid metabolism. Nature. 2009Apr30 458;(7242)1131–1135.
[7] Sinha RA, You SH, Zhou J, et al. Thyroid hormone stimulates hepatic lipid catabolism via activation of autophagy. J Clin Invest. 2012 Jul;122(7):2428–2438.
[8] Baek SH, Kim KI. Epigenetic control of autophagy: nuclear events gain more attention. Mol Cell. 2017Mar2; 65(5):781–785.
[9] Fullgrabe J, Klionsky DJ, Joseph B. The return of the nucleus: transcriptional and epigenetic control of autophagy. Nat Rev Mol Cell Biol. 2014 Jan;15(1):65–74.

[10] Fullgrabe J, Ghislat G, Cho DH, et al. Transcriptional regulation of mammalian autophagy at a glance. J Cell Sci. 2016Aug15 129; (16)3059–3066.

[11] Shin HJ, Kim H, Oh S, et al. AMPK-SKP2-CARM1 signalling cascade in transcriptional regulation of autophagy. Nature. 2016Jun23 534;(7608)553–557.

[12] Sardiello M, Palmieri M, Di Ronza A, et al. A gene network regulating lysosomal biogenesis and function. Science. 2009Jul24 325;(5939)473–477.

[13] Settembre C, Di Malta C, Polito VA, et al. TFEB links autophagy to lysosomal biogenesis. Science. 2011Jun17 332;(6036)1429–1433.

[14] Settembre C, De Cegli R, Mansueto G, et al. TFEB controls cellular lipid metabolism through a starvation-induced autoregulatory loop. Nat Cell Biol. 2013 Jun;;15(6):647–658.

[15] Lee JM, Wagner M, Xiao R, et al. Nutrient-sensing nuclear receptors coordinate autophagy. Nature. 2014Dec4 516;(7529)112–115.

[16] Seok S, Fu T, Choi SE, et al. Transcriptional regulation of autophagy by an FXR-CREB axis. Nature. 2014Dec4 516;(7529) 108–111.

[17] Sinha RA, Singh BK, Zhou J, et al. Thyroid hormone induction of mitochondrial activity is coupled to mitophagy via ROS-AMPK-ULK1 signaling. Autophagy. 2015;11(8):1341–1357.

[18] Sinha RA, Singh BK, Yen PM. Direct effects of thyroid hormones on hepatic lipid metabolism. Nat Rev Endocrinol. 2018 May;14 (5):259–269.

[19] Chen W, Roeder RG. Mediator-dependent nuclear receptor function. Semin Cell Dev Biol. 2011 Sep;22(7):749–758.

[20] Yuan CX, Ito M, Fondell JD, et al. The TRAP220 component of a thyroid hormone receptor- associated protein (TRAP) coactivator complex interacts directly with nuclear receptors in a ligand-dependent fashion. Proc Natl Acad Sci U S A. 1998Jul7 95; (14)7939–7944.

[21] Javitt NB. Hep G2 cells as a resource for metabolic studies: lipoprotein, cholesterol, and bile acids. Faseb J. 1990Feb1; 4(2):161–168.

[22] Bjorkoy G, Lamark T, Pankiv S, et al. Monitoring autophagic degradation of p62/SQSTM1. Methods Enzymol. 2009;452:181–197.

[23] Klionsky DJ, Abdalla FC, Abeliovich H, et al. Guidelines for the use and interpretation of assays for monitoring autophagy. Autophagy. 2012 Apr;8(4):445–544.

[24] Kimura S, Noda T, Yoshimori T. Dissection of the autophagosome maturation process by a novel reporter protein, tandem fluorescent-tagged LC3. Autophagy. 2007 Sep-Oct;3(5):452–460.

[25] nsSingh BK, Sinha RA, Tripathi M, et al. Thyroid hormone receptor and ERRalpha coordinately regulate mitochondrial fission, mitophagy, biogenesis, and function. Sci Signal. 2018Jun26;11:536.

[26] Lachmann A, Xu H, Krishnan J, et al. ChEA: transcription factor regulation inferred from integrating genome-wide ChIP-X experiments. Bioinformatics. 2010Oct1 26;(19)2438–2444.

[27] Zhu Y, Qi C, Jain S, et al. Isolation and characterization of PBP, a protein that interacts with peroxisome proliferator-activated receptor. J Biol Chem. 1997Oct10 272;(41)25500–25506.

[28] Son YL, Lee YC. Molecular determinants of the interactions between LXR/RXR heterodimers and TRAP220. Biochem Biophys Res Commun. 2009Jul3; 384(3):389–393.

[29] Kaya Okur HS, Das A, Taylor RN, et al. Roles of estrogen receptor-alpha and the coactivator MED1 during human endometrial decidualization. Mol Endocrinol. 2016 Mar;30(3):302–313.

[30] Peeters JGC, Picavet LW, Coenen S, et al. Transcriptional and epigenetic profiling of nutrient-deprived cells to identify novel regulators of autophagy. Autophagy. 2019 Jan;15(1):98–112.

[31] Xiang J, Liu X, Ren J, et al. How does estrogen work on autophagy? Autophagy. 2019 Feb;15(2):197–211.

[32] Jegga AG, Schneider L, Ouyang X, et al. Systems biology of the autophagy-lysosomal pathway. Autophagy. 2011 May;7(5):477–489.

[33] The Foxo-autophagy CZ. Axis in health and disease. Trends Endocrinol Metab. 2019 Sep;30(9):658–671.

[34] Widjaja AA, Singh BK, Adami E, et al. Inhibiting interleukin 11 signaling reduces hepatocyte death and liver fibrosis, inflammation, and steatosis in mouse models of nonalcoholic steatohepatitis. Gastroenterology. 2019 Sep;157(3):777–792 e14.

[35] Lipinski MM, Hoffman G, Ng A, et al. A genome-wide siRNA screen reveals multiple mTORC1 independent signaling pathways regulating autophagy under normal nutritional conditions. Dev Cell. 2010Jun15 18;(6)1041–1052.

[36] Settembre C, Zoncu R, Medina DL, et al. A lysosome-to-nucleus signalling mechanism senses and regulates the lysosome via mTOR and TFEB. Embo J. 2012Mar7 31;(5)1095–1108.

[37] Liu HY, Han J, Cao SY, et al. Hepatic autophagy is suppressed in the presence of insulin resistance and hyperinsulinemia: inhibition of FoxO1-dependent expression of key autophagy genes by insulin. J Biol Chem. 2009 Nov6 284;(45) 31484–31492.

[38] Ezaki J, Matsumoto N, Takeda-Ezaki M, et al. Liver autophagy contributes to the maintenance of blood glucose and amino acid levels. Autophagy. 2011 Jul;7(7):727–736.

[39] Waskowicz LR, Zhou J, Landau DJ, et al. Bezafibrate induces autophagy and improves hepatic lipid metabolism in glycogen storage disease type Ia. Hum Mol Genet. 2019Jan1 28;(1) 143–154.

[40] Zhou J, Waskowicz LR, Lim A, et al. A liver-specific thyromimetic, VK2809, decreases hepatosteatosis in glycogen storage disease type ia. Thyroid. 2019 Aug;29(8):1158–1167.

[41] Fondell JD. The mediator complex in thyroid hormone receptor action. Biochim Biophys Acta. 2013 Jul;1830(7):3867–3875.

[42] Jia Y, Qi C, Kashireddi P, et al. Transcription coactivator PBP, the peroxisome proliferator-activated receptor (PPAR)-binding protein, is required for PPARalpha-regulated gene expression in liver. J Biol Chem. 2004Jun4 279;(23)24427–24434.

[43] Kabeya Y, Mizushima N, Ueno T, et al. LC3, a mammalian homologue of yeast Apg8p, is localized in autophagosome membranes after processing. Embo J. 2000Nov1 19;(21) 5720–5728.

[44] Zhou J, Farah BL, Sinha RA, et al. Epigallocatechin-3-gallate (EGCG), a green tea polyphenol, stimulates hepatic autophagy and lipid clearance. PLoS One. 2014;9(1):e87161.

[45] Denis RG, Joly-Amado A, Webber E, et al. Palatability can drive feeding independent of AgRP neurons. Cell Metab. 2015Oct6 22; (4)646–657.